Available online at www.sciencedirect.com
SCIENCE DIRECT
Journal of Photochemistry and Photobiology A: Chemistry 174 (2005) 171–179
Journal of Photochemistry and Photobiology A:Chemistry
www.elsevier.com/locate/jphotochem

Influence of the properties of TiO_2 particles on a photocatalytic acrylate polymerisation

C. Damm [a,*], D. Völtzke [b], H.-P. Abicht [b], G. Israel [c]

[a] *University Erlangen-Nuremberg, Institute of Polymer Materials, Martensstrasse 7, 91058 Erlangen, Bavaria, Germany*
[b] *Martin-Luther-University of Halle-Wittenberg, Department of Inorganic Chemistry, Kurt-Mothes-Strasse 2, 06120 Halle/Saale, Germany*
[c] *Martin-Luther-University of Halle-Wittenberg, Department of Organic Chemistry, Kurt-Mothes-Strasse 2, 06120 Halle/Saale, Germany*

Received 14 December 2004
Available online 12 April 2005

Abstract

Samples of TiO_2 having different BET surface areas and different numbers of primary crystallites per secondary particle were prepared by annealing amorphous TiO_2 at different temperatures.

The photocatalytic activity of these TiO_2 samples was checked using the polymerisation of a trisacrylate as test reaction. Amorphous TiO_2 is not able to initiate the polymerisation of the trisacrylate used. The maximum polymerisation rate as well as the monomer conversion after an illumination time of 120 s increases with increasing number of primary crystallites per particle. That means it increases with increasing grain boundary area inside the secondary particles.

To get a better understanding of the photocatalytic properties the photoelectric primary processes in the TiO_2 samples were investigated using measurements of the transient photoelectromotive force (Photo-EMF).

Amorphous TiO_2 does not show any Photo-EMF signal. This means illumination does not generate mobile charge carriers. For this reason, in the case of amorphous TiO_2 no photocatalytic activity may be expected.

The maximum Photo-EMF of TiO_2 as a measure of the efficiency of charge separation increases with increasing number of primary crystallites per particle. A direct correlation between the maximum Photo-EMF U_{max} and the maximum rate of the acrylate photopolymerisation r_p^{max} shows that the photoelectric primary processes in the catalyst are of great importance for its photocatalytic activity.

Keywords: TiO_2; Particle properties; Photoelectromotive force (Photo-EMF); Photopolymerisation

1. Introduction

In recent years, increasing attention has been paid to heterogeneous photocatalysis. Besides basic research some applications in purification of waste water and air were presented [1–7].

Most papers in the field of heterogeneous photocatalysis deal with the degradation or mineralization of organic compounds as halogenated compounds [8–12], dyes [13–18] or polymers [19–21]. A smaller number of papers reports about photocatalytic syntheses of organic compounds [22,23], initiation of polymerisation [24–28] or the recovery of noble metals [29–31].

TiO_2 which may exist in the crystalline modifications anatase and rutile or in an amorphous form is the most popular photocatalyst material. In [9,17,18,31–33], it was shown that the photocatalytic activity of anatase is much higher than that of rutile or amorphous TiO_2. The photocatalytic activity of semicrystalline TiO_2 samples increases with increasing anatase content [9].

Other structural properties like grain size, doping, adsorption of metal ions or deposition of metals influence the photocatalytic activity of a photoconducting material as well [10,13,16,18,20,23,31,34].

* Corresponding author. Tel.: +49 9131 85 27748; fax: +49 9131 85 28321.
E-mail addresses: cornelia.damm@ww.uni-erlangen.de (C. Damm), voeltzke@chemie.uni-halle.de (D. Völtzke), abicht@chemie.uni-halle.de (H.-P. Abicht), israel@chemie.uni-halle.de (G. Israel).

1010-6030/$ – see front matter © 2005 Elsevier B.V. All rights reserved.
doi:10.1016/j.jphotochem.2005.03.006

Generally, a heterogeneous photocatalytic reaction consists of two steps: firstly due to illumination the generation, diffusion, and recombination of charge carriers within the catalyst material. These reactions were summarized as photoelectric primary process. The second step is the charge transfer through the catalyst surface and the succeeding chemical transformation of the adsorbed reactant.

The photoelectric primary process may be very important for the efficiency of the photocatalytic process. For that reason the results of heterogeneous photocatalysis experiments must be discussed both on the basis of the crystallographic structure and the photoelectric properties of the catalyst materials. Until now only a few authors did combine preparative or mechanistic investigations of heterogeneous photocatalytic reactions with measurements of the photoelectric properties of the same material used as photocatalyst [12,15,16,21,24].

In this paper, we report about the heterogeneous photocatalytic polymerisation of a trisacrylate ester using TiO_2 samples as a catalyst having different numbers of primary crystallites per particle as well as different BET surface areas. The samples were prepared by spray hydrolysis [38]. For comparison the commercial photocatalyst P25 (Degussa AG) as well as commercial anatase pigment produced by Merck are investigated too.

The photoelectric primary processes in the TiO_2 samples are characterized using measurements of transient photoelectromotive force (Photo-EMF). Combining photopolymerisation and Photo-EMF measurements, we are able to demonstrate the great importance of the photoelectric properties for the heterogeneous photocatalytic reaction.

Because not widely used the Photo-EMF method shall be introduced briefly.

To perform Photo-EMF measurements the sample is brought into a capacitor. A laser flash (pulse duration 300 ps) illuminates the sample through a transparent electrode. Due to the laser impulse at the surface of the sample electrons (e^-) are excited from the valence band (VB) into the conduction band (CB). They leave at the VB positive holes (h^+). After the laser flash both charge carriers move into the bulk of photoconductor along the direction of incident light driven by their concentration gradient. A charge separation takes place at phase boundaries, structural defects and at chemical impurity or dopant sites if the electrons and holes have different mobility. Titanium dioxide is a n-type photoconductor. This means that the concentration of electrons is higher than that of the holes. With most semiconductor materials, also the mobility of electrons is usually higher than that of holes. As a result mainly electrons reach the bulk of the pigment. The spatial charge separation creates a photo-induced potential which can be measured as photoelectromotive force.

The transient photovoltage is measured contactless and without any external electric field as a function of the time. For that reason the charge carrier concentration gradient due to the gradient of light absorption and heterojunctions within the sample are the only driving forces for the Photo-EMF generation. So this method is well suited for investigations of materials structures on their photoelectric properties [35].

From the sign of a Photo-EMF signal the type of photoconductor can be deduced. Materials behave as n-type photoconductors show Photo-EMF signals with positive sign. If the signal shows a crossing point with the zero potential the photoconductor type can be derived from the sign at the beginning of the decay process.

The amount of the maximum Photo-EMF U_{max} upon illumination is a measure of the efficiency of charge generation and separation.

After illumination the Photo-EMF decreases due to recombination or chemical reactions of the charge carriers. For the description of the Photo-EMF decay we use a biexponential rate law, see Eq. (1).

$$U(t) = U_1^0 \exp(-k_1 t) + U_2^0 \exp(-k_2 t) \quad (1)$$

Per definition the process with the parameters U_1^0 and k_1 always is the faster decay process. That means $k_1 > k_2$.

The cause of the biexponential decay behaviour of the Photo-EMF is a generation of two partial Photo-EMFs decaying independently. The partial voltages U_1^0 and U_2^0 are the values of both Photo-EMFs at the beginning of their decay process, k_1 and k_2 are their first order decay constants. The sum of U_1^0 and U_2^0 is U_{max}.

In our previous work, we have shown that a generation of a Photo-EMF in the subsurface region additional to the DEMBER-EMF in the bulk causes the biexponential Photo-EMF decay. Usually the trap concentration in the surface and subsurface regions are higher than in the bulk resulting in band bendings in the surface region. So additional to the DEMBER Photo-EMF in the bulk a second one is generated in the surface and subsurface region due to band bendings. If both Photo-EMFs are opposite directed the sum of them may show a zero potential passage. That means the biexponential Photo-EMF decay is a property of pure photoconductors. According to the findings of our previous works we are able to assign the faster decay process (parameters U_1^0, k_1) to a Photo-EMF in the subsurface region of the catalyst particles [36,37]. That means U_1^0 represents a charge carrier amount in the subsurface region, k_1 is a measure of the recombination rate in the surface and subsurface region. The parameters U_2^0 and k_2 represent the initial amount of charge carriers and their recombination rate in the bulk of the sample.

In [21,36], the Photo-EMF method is described more in detail.

2. Experimental

2.1. Materials

Anatase pigment, titanium-tetraisopropoxide, dichlormaleic acid anhydride, and 1,2-dichlorethane were purchased from Merck Darmstadt.

Table 1
Phase content, primary crystallite size, specific surface area and particle size of TiO_2 samples nos. 1–6 used in this work

Sample no.	TiO_2 sample	Phase	Primary crystallite size (nm)	BET surface area (m^2/g)	Particle size according to BET (nm)	No. of primary crystallites per particle
1	As prepared	Amorphous	0	360	–	–
2	350 °C/2 h	Anatase	23	35.3	43	2
3	600 °C/2 h	Anatase	30	5.9	261	9
4	450 °C/24 h + 600 °C/3 h	Anatase	30	3.1	498	17
5	TiO_2 (Merck)	Anatase	49	8.8	186	4
6	Photocatalyst P25	75% Anatase + 25% Rutile	22 (Anatase) 33 (Rutile)	50	30	1

According to the supplier the anatase pigment contains up to 0.005 wt.% Fe^{3+} and up to 0.002 wt.% Cr^{3+} as impurities. The titanium-tetraisopropoxide has a purity larger than 98%, the main impurity is isopropanole.

TiO_2 photocatalyst P25 was purchased from Degussa AG. The deliverer checked the purity of P25 by atomic absorption spectroscopy: P25 contains up to 0.007 wt.% Fe^{3+} but no other critical metal ions as impurity.

The polyvinyl-butyrale used as matrix for the Photo-EMF measurements was produced by Wacker Burghausen. All materials were used as received without further purification.

The trisacrylate monomer used was purchased from Cray Valley. Before use the inhibitors were removed by filtration over Al_2O_3.

2.2. Preparation of the TiO_2 samples

The TiO_2 samples were prepared by spray hydrolysis of titanium-tetraisopropoxide using a modified spray dryer Büchi B-191 (Büchi GmbH). More details of the preparation process are given in [38].

The as-prepared material (sample no. 1, see Table 1) was annealed at 350 or 600 °C for 2 h, respectively (samples nos. 2 and 3, respectively, see Table 1). One TiO_2 sample was heated firstly for 24 h at 450 °C followed by 3 h heating at 600 °C (sample no. 4, see Table 1). For annealing a muffle furnace was used. All annealing processes were carried out in air.

2.3. Morphology of the TiO_2 samples

The morphology of the TiO_2 samples was investigated by scanning electron microscopy (SEM) using a LEO 430 (Zeiss, Leica). For SEM investigations, gold was deposited on the powder samples.

2.4. Specific surface area

The specific surface area of the TiO_2 powders was determined by N_2 adsorption at 77 K (BET method) using a high speed gas sorption analyzer (Quantachrome). The BET specific surfaces were used to calculate the average particle sizes assuming the existence of spherical particles with a monomodal size distribution.

2.5. X-ray diffraction

Powder X-ray diffraction (XRD) was used to determine the crystal structure as well as the sizes of the primary crystallites. The X-ray diffraction pattern were recorded in the range of 2Θ between 20 and 70° using Cu $K\alpha_1$ irradiation (STOE, StadiP MP).

2.6. EPR investigations

Q-band EPR spectra (BRUKER, 34.2 GHz) were recorded at room temperature using TiO_2 powder samples.

2.7. Photo-EMF measurements

Photo-EMF measurements were performed using pigment polymer dispersion layers. To prepare samples for the Photo-EMF measurements, 100 mg of TiO_2 were dispersed in 3 g of a solution of polyvinyl butyrale in 1,2-dichlorethane (10 wt.%) using a one ball vibrating mill.[1] The mixture was cast on a glass slide (area, 47.6 cm^2) and dried in a solvent atmosphere. After 48 h the layer was removed from the glass and dried for 8 h in vacuum at room temperature before use.

The layers had a thickness of about 60–80 μm and a total absorption in the UV range.

Pieces having a diameter of 10 mm were cut from the layers and brought into the Photo-EMF device.

The sample was illuminated by a single flash of a nitrogen laser PNL 100; Lasertechnik Berlin GmbH (wavelength, 337 nm; pulse duration, 300 ps; power, 100 kW). The energy of the actinic light pulse was about 3×10^{13} quanta per flash at the sample's place. The temperature of the sample and the amplifier was 25 °C.

All Photo-EMF signals and parameters presented here are the mean values of three measurements. Each measurement was performed using a new piece of the sample.

The Photo-EMF device is constructed like a capacitor with a transparent NESA glass as measuring electrode and a grounded metal plate on the rear side of the sample. The transient Photo-EMF is measured contactless using insulating foils between the sample and the electrodes. No external electric field is applied. For more details see [36].

[1] Processing conditions: 30 min milling at room temperature.

2.8. Photopolymerisation

The light induced polymerisation of the trisacrylate 1 is used to investigate the photocatalytic activity of the TiO_2 sample nos. 1–6, see Table 1. The 6.5 mol% related to monomer of the added electron acceptor dichloromaleic acid anhydride 2 will provide an electron/hole symmetry over a long period of the photocatalytic initiation reaction.

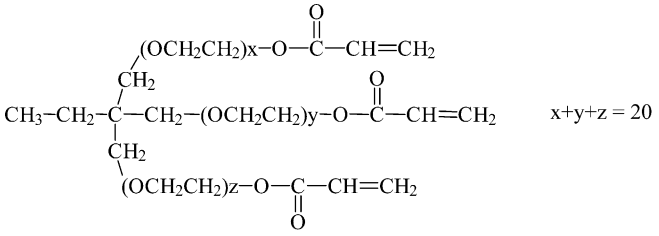

1

The samples contained 5.5 wt.% of the respective TiO_2 powder under investigation. For comparison the mixture was also irradiated without any added TiO_2 catalyst (curve 0, see Fig. 4).

To disperse the TiO_2 powder in the monomer the same milling procedure as described in Section 2.7 was used.

The polymerisation experiments were performed using a film of the pigment-monomer mixture, $d = 20\ \mu m$, and cast with a knifecoater.

The layers were illuminated with white light of a 100-W mercury high pressure lamp with an intensity of 90 mW/cm^2 at the sample's place. To avoid a direct excitation of the acrylate monomer all radiation below 350 nm was removed using a cut-off glass filter (Schott).

The relative concentration of double bonds was determined by real time infrared spectroscopy RT-FTIR with a spectrometer "FTS6000" (Biorad) monitoring the absorption band at 810 cm^{-1} (C=C–H wagging vibration) of the acrylate monomer as a function of the illumination time.

To exclude oxygen the sample chamber of the spectrometer was flushed with nitrogen 3 min before as well as during the whole irradiation time.

The results of all polymerisation experiments presented here are mean values of three attempts.

3. Results and discussion

3.1. Structure of the samples

The TiO_2 as prepared by spray hydrolysis (sample no. 1) does not show any X-ray diffraction peak indicating an amorphous material. The annealed materials (samples no. 2–4) as well as the sample produced by Merck (sample no. 5) show a X-ray diffraction peak at $2\theta = 25.28^\circ$ which is the (1 0 1) peak of the anatase type. The intensity of this peak increases in the following order: annealed at 350 °C/2 h (sample no. 2) < annelead at 600 °C/2 h (sample no. 3) < Merck anatase (sample no. 5) < annealed at 450 °C/24 h + 600 °C/3 h (sample no. 4).

The TiO_2 photocatalyst P25 (sample no. 6) exhibits an additional peak at $2\theta = 27.45^\circ$ which is the (1 1 0) peak of the rutile type. From the integral peak intensities the amounts of anatase and rutile were calculated to 75 and 25%, respectively, (see Table 1).

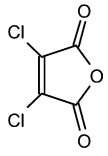

2

Using the Scherrer equation and assuming a spherical shape of the primary crystallites their mean size can be calculated from the full line width at half-maximum height (FWHM) of the (1 0 1) and the (1 1 0) XRD diffraction peak. The results are shown in Table 1. The primary crystallite sizes in the samples prepared by spray hydrolysis (sample nos. 2–4) and in the photocatalyst P25 (sample no. 6) are similar, they are in the range between 20 and 30 nm. The annealing temperature has no noticeable influence on the primary crystallite size. The TiO_2 produced by Merck (sample no. 5) has larger primary crystallites (about 50 nm).

Additionally, Table 1 shows the values for the specific surface area of the samples and the particles size calculated from that.

Annealing of the amorphous TiO_2 leads to a dramatic decrease of the specific surface area. This means small particles agglomerate to larger ones. The average number of primary crystallites per particle increase with increasing annealing temperature. That means samples annealed at higher temperatures contain more grain boundaries inside the secondary particles than samples annealed at lower temperatures. In comparison to the self-prepared crystalline TiO_2 samples, the specific surface area of the commercial photocatalyst P25 is much higher, and one particle consists virtually of one primary crystallite in the simple morphological model used here. Because the surface area of a photocatalyst plays an important role in the heterogeneous photocatalytic process, a higher photocatalytic activity may be expected for P25 (sample no. 6).

Fig. 1a shows the SEM micrograph of the TiO_2 sample prepared by spray hydrolysis after annealing at 600 °C/2 h. The micrograph shows the typical morphology for all self-prepared, spray-hydrolysed TiO_2 samples. This morphology is characterized by the existence of dented hollow spheres in the size range of 5–10 μm. These hollow spheres, representing the original droplets, are agglomerates of more or less small primary particles (crystallites) as can be seen from the

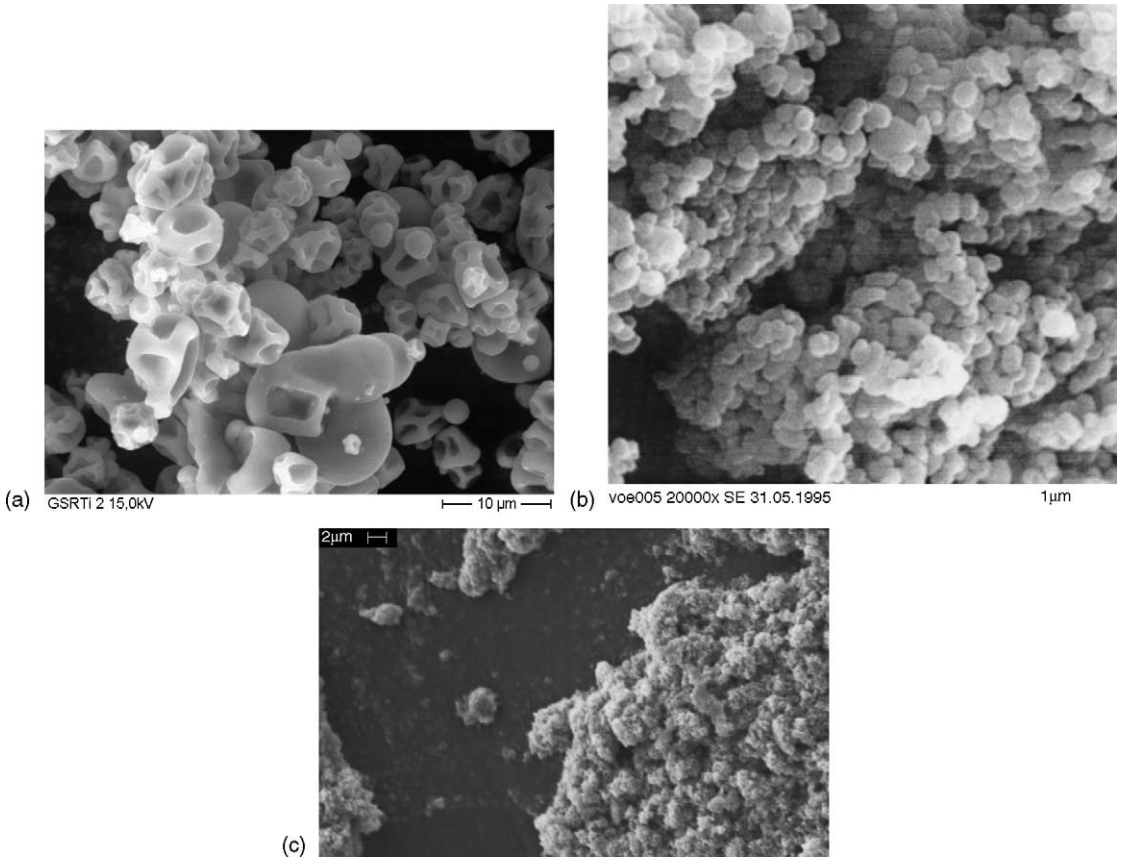

Fig. 1. (a) SEM micrograph of a TiO_2 sample prepared by spray hydrolysis and annealed at 600 °C/2 h (sample no. 3). (b) SEM micrograph of TiO_2 produced by Merck (sample no. 5). (c) SEM micrograph of the TiO_2 photocatalyst P25 (sample no. 6).

BET surfaces, Table 1. Changing the annealing conditions will influence the crystallite size.

Fig. 1b and c show SEM micrographs of the TiO_2 sample nos. 5 and 6, respectively. The Merck product (Fig. 1b) is characterized by crystallites sizing in the range far below 1 μm. Fig. 1c reveals that the photocatalyst P25 also consists of agglomerates (about 3 μm in diameter) of smaller particles.

To check if the samples contain paramagnetic impurities solid state EPR measurements were performed.

The spectrum of the TiO_2 Merck, sample no. 5, shows two signals. Their *g* factors 1.9993 and 1.9666, respectively, correspond to signals typical for Fe^{3+} and Cr^{3+}, see (Fig. 2). The samples prepared by spray hydrolysis do not show any impurity-like EPR signal. That means the contents of these impurities are much lesser than in the TiO_2 produced by Merck.

This finding proofs a doping of the TiO_2 Merck, no. 5, by Fe^{3+} and Cr^{3+} ions.

To get more information about the doping level of TiO_2 Merck a X-ray fluorescence analysis was performed: this sample contains 0.34 wt.% Al_2O_3, 0.22 wt.% SiO_2, 0.57 wt.% P_2O_5, 0.1 wt.% K_2O, 0.02 wt.% CaO, 0.14 wt.% Cr_2O_3, 0.04 wt.% ZrO_2 and 0.04 wt.% Nb_2O_5. This analysis shows that the supplier's information about impurities is incomplete. This TiO_2 is a heavily doped material. For a material like TiO_2 Merck is known from literature that the Fe^{3+} and Cr^{3+} ions occupy places in the Ti(IV) lattice if their contents are below 1 wt.% [14–16].

Based on the results shown in this chapter, the TiO_2 samples investigated in this work can be classified as follows:

(i) amorphous TiO_2, undoped (sample no. 1);
(ii) pure anatase polymorph, undoped (sample nos. 2–4);
(iii) pure anatase polymorph, heavily doped and probably partially coated by barrier layers (sample no. 5);
(iv) heterojunction of the TiO_2 polymorphs anatase and rutile (sample no. 6).

3.2. Photoelectric properties

Fig. 3 shows the Photo-EMF signals of the different TiO_2 sample nos. 1–6. The maximum values U_{max} and the kinetic parameter of the Photo-EMF of the TiO_2 samples investigated are summarized in Table 2.

The results shown in Fig. 3 and Table 2 may be summarized and discussed as follows.

The as-prepared amorphous TiO_2, sample no. 1, does not show any Photo-EMF signal. This means illumination of this sample does not lead to charge carrier generation. For that

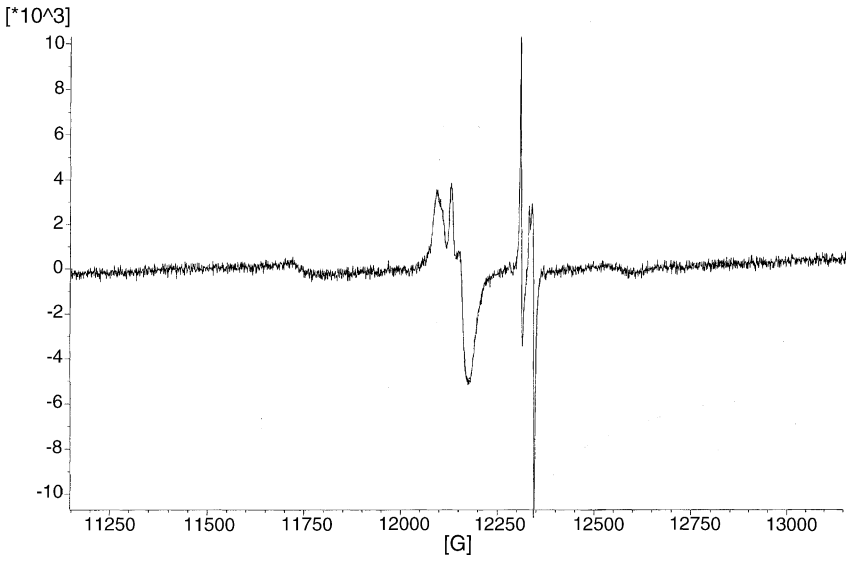

Fig. 2. Solid state EPR spectrum of the TiO_2 sample (Merck), no. 5.

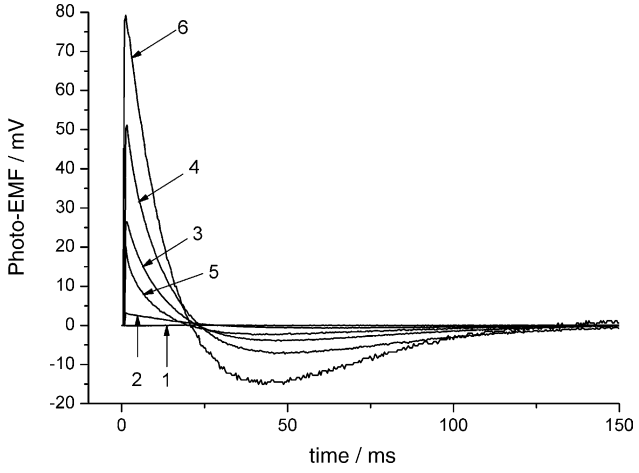

Fig. 3. Photo-EMF signals of the TiO_2 samples nos. 1–6: curve 1, line at $U = 0$, as-prepared (amorphous) TiO_2 (sample no.1); curve 2, 350 °C/2 h (sample no. 2); curve 3, 600 °C/2 h (sample no. 3); curve 4, 450 °C/24 h + 600 °C/3 h (sample no. 4); curve 5, TiO_2 Merck (sample no. 5); curve 6, photocatalyst P25 (sample no. 6).

reason no photocatalytic activity may be expected although the specific surface area is high.

The undoped anatase sample nos. 2–4, the doped anatase sample Merck, no. 5, as well as the anatase-rutile-heterostructure P25, no. 6, show Photo-EMF signals with zero passage starting with a positive sign. According to our previous studies such signals are typical for n-type photoconductors [36].

The cause for the zero passages in the Photo-EMF signals are differences in the photoelectric properties of the subsurface and bulk region, see Section 1. Zero passages in the Photo-EMF signals can also be obtained by admixing a p-type material to a n-type photoconductor. But undoped rutile is also a n-type photoconductor. For that reason small amounts of rutile in the anatase samples cannot be the reason for the zero passages in the Photo-EMF signals. Moreover, in that case the zero passage should be more pronounced in P25 than in the other samples because of its higher rutile content. But this is not observed, see Fig. 3.

The maximum Photo-EMF which is a measure of the efficiency of charge separation increases strongly with increasing average number of primary crystallites per particle. That means grain boundaries inside the secondary particles favourite the charge separation. The anatase-rutile-heterostructure P25, no. 6, shows the highest U_{max} value because the heterojunction between the anatase and rutile polymorph enhances the charge separation. The doped anatase sample (Merck), no. 5, shows a U_{max} value which is much smaller than that of the sample heated to 600 °C/2 h (sample no. 3) although the particle sizes calculated from BET surface area are comparable for both samples. The reasons for this

Table 2
Maximum values U_{max} and kinetic parameters of the Photo-EMF signals shown in Fig. 3

Curve no. in Fig. 3	TiO_2 sample	U_{max} (mV)	U_1^0 (V)	U_2^0 (V)	k_1 (s^{-1})	k_2 (s^{-1})
1	As prepared (sample 1)	0	0	0	–	–
2	350 °C/2 h (sample 2)	3.2 ± 0.5	0.901 ± 0.131	−0.898 ± 0.130	32.6 ± 0.6	32.4 ± 0.6
3	600 °C/2 h (sample 3)	26.8 ± 3.0	2.610 ± 1.887	−2.583 ± 1.884	42.9 ± 0.3	42.3 ± 0.3
4	450 °C/24 h + 600 °C/3 h (sample 4)	52.2 ± 1.5	5.520 ± 2.512	−5.468 ± 2.510	41.4 ± 0.2	40.9 ± 0.3
5	TiO_2 (Merck) (sample 5)	20.2 ± 3.4	0.045 ± 0.005	−0.024 ± 0.006	63.9 ± 3.8	33.5 ± 4.2
6	P25 (sample 6)	79.2 ± 2.2	8.424 ± 1.209	−8.345 ± 1.208	35.9 ± 1.7	35.7 ± 1.7

difference are doping effects as well as fewer grain boundaries in the TiO_2 (Merck). The Fe^{3+} and Cr^{3+} ions occupying lattice places may act as recombination centres leading to an enhanced annihilation of charge carriers.

Because the charge separation is an important primary step in the heterogeneous photocatalytic process it may be expected that the photocatalytic activity of the samples increases with increasing $U_{max.}$ For that reason it should increase with increasing number of grain boundaries per particle. The photocatalyst P25, no. 6., should show the highest activity. The TiO_2 (Merck) no. 5, as well as sample no. 2 should show only low activity.

For all crystalline TiO_2 samples the partial Photo-EMFs U_1^0 and U_2^0 have opposite signs. In the most cases the amounts of U_1^0 and U_2^0 are very similar. The amounts of U_1^0 and U_2^0 change with the structure of the samples in the same direction as U_{max}.

The Photo-EMF decay constants k_1 and k_2 are relative measures of the recombination rate and therefore for the charge carrier lifetimes in the subsurface and in the bulk region of the photocatalyst particles, respectively.

In the undoped anatase samples (nos. 2–4) as well as in the anatase-rutile heterostructure (no. 6) the values for k_1 and k_2 are comparable but k_1 and k_2 are not equal, see Table 2. If $k_1 = k_2$ the Photo-EMF decay would be first order and no zero passage should be observed. The very small differences in the values of k_1 and k_2 are sufficient to cause a signal showing a zero passage.

Only for the doped anatase (Merck), no. 5, there k_1 is noticeable higher than k_2. This means that here the photoelectric properties of the subsurface region differ strong from that of the bulk. The reason for this may arise from simple aging or more probably from surface coating within the preparation procedure. But according to IR experiments an organic coating can be excluded. So the coating must be an inorganic material not detectable by IR spectroscopy. A SiO_2 and/or Al_2O_3 coating of TiO_2 pigments which are used for paints or as fillers for polymers is known to suppress their photocatalytic activities [20]. Indeed the presence of Al_2O_3 and SiO_2 can be proven by X-ray fluorescence analysis. Doping of TiO_2 by Al^{3+}, substituting Ti^{4+} renders TiO_2 a p-type semiconductor as proved for rutile by Yahia and others. But our Photo-EMF results demonstrate, however, that the material is n-type. This is another argument why Al_2O_3 in TiO_2 Merck should cover the crystal surface as a partial coat.

A comparison of the k_1 values shows that the value for the doped anatase, no. 5, is highest one. This means, that in TiO_2 (Merck), no. 5, the surface recombination rate is faster than in the other samples. But, for an effective photocatalytic reaction a sufficient lifetime of charge carriers in the surface and subsurface region is necessary. Thus, the doped TiO_2 produced by Merck should show the lowest photocatalytic activity.

It is shown that doping of anatase with Fe^{3+} or Cr^{3+} in the concentration range between 0.1 and 10 mol% results in a decrease of the charge carrier lifetimes, [14,16], and therefore in an increasing Photo-EMF decay rate. The influence of Fe^{3+} or Cr^{3+} doping on the maximum Photo-EMF U_{max} of TiO_2 is not discussed explicitely in [14,16]. But it may be expected that doping influences U_{max} too.

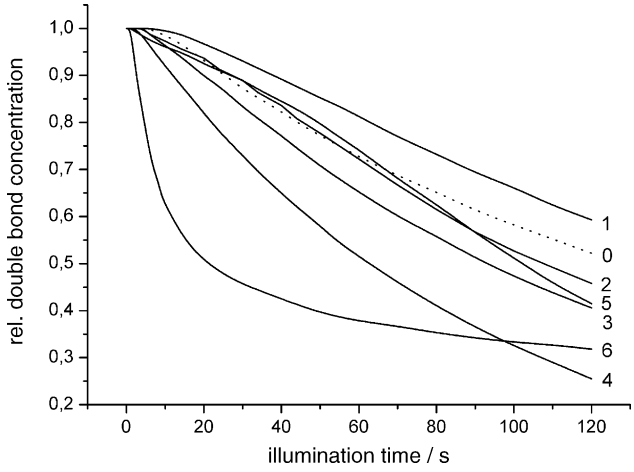

Fig. 4. Kinetics of the photopolymerisation of the acrylate 1 pigmented with 5.5 wt.% of the different TiO_2 samples nos. 1–6 (solid lines): curve 1, as prepared (sample No. 1); curve 2, 350 °C/2 h (sample no. 2); curve 3, 600 °C/2 h (sample no. 3); curve 4, 450 °C/24 h + 600 °C/3 h (sample no. 4); curve 5, TiO_2 Merck (sample no. 5); curve 6, photocatalyst P25 (sample no. 6); curve 0, acrylate mixture without any TiO_2 photocatalyst, but in the presence of the electron acceptor 2.

3.3. Photopolymerisation

Fig. 4 shows the relative concentration of double bonds as a function of the illumination time from samples containing the acrylate 1, the electron acceptor 2 and the TiO_2 samples mentioned. The kinetics of the blank sample is shown also.

The maximum polymerisation rate r_P^{max} was determined by differentiating the curves shown in Fig. 4. Moreover the conversion degree of double bonds after an illumination time of 120 s, $C_{120\,s}$, was determined from the experimental curves. The results are summarized in Table 3.

All in all the results shown in Fig. 4 and Table 3 confirm the hypotheses about the photocatalytic activities of the TiO_2 samples stated in the Section 3.2. The mixtures containing as-prepared amorphous TiO_2 (sample no. 1) polymerises slower than the acrylate without TiO_2. This means the as-prepared TiO_2 is not able to initiate the polymerisation by any own photocatalytic activity. But it acts as an internal light filter and hence inhibits partially the polymerisation.

The polymerisation rate of the sample containing the doped anatase (Merck), no. 5, is comparable with that of a mixture without TiO_2. That means the TiO_2 (Merck), no. 5, shows no noticeable photocatalytic activity as it was expected from the Photo-EMF kinetics and the rather low maximum Photo-EMF.

The poor photocatalytic activity of the TiO_2 (Merck), no. 5, is caused by the presence of Fe^{3+} and Cr^{3+} impurities. In [14,16] was shown that doping TiO_2 with Fe^{3+} or Cr^{3+}

Table 3
Maximum rate of the photopolymerisation r_p^{max} and double bond conversion after 120 s illumination C_{120s} of the acrylate samples mentioned in Fig. 4

Curve no. in Fig. 4	Sample	r_P^{max}/M_0 (s^{-1})	$C_{120\,s}$ (%)
0	Without TiO_2	$(6.0 \pm 0.3) \times 10^{-3}$	47.8 ± 2.4
1	As prepared (TiO_2 sample no. 1)	$(4.2 \pm 0.2) \times 10^{-3}$	40.7 ± 2.0
2	350 °C/2 h (TiO_2 sample no. 2)	$(5.9 \pm 0.3) \times 10^{-3}$	54.2 ± 2.7
3	600 °C/2 h (TiO_2 sample no. 3)	$(6.6 \pm 0.3) \times 10^{-3}$	59.4 ± 3.0
4	450 °C/24 h + 600 °C/3 h (TiO_2 sample no. 4)	$(1.1 \pm 0.1) \times 10^{-2}$	74.5 ± 3.7
5	TiO_2 Merck (TiO_2 sample no. 5)	$(5.8 \pm 0.3) \times 10^{-3}$	58.5 ± 2.9
6	P25 (TiO_2 sample no. 6)	$(5.7 \pm 0.3) \times 10^{-2}$	68.1 ± 3.4

ions may decrease the rate of a photocatalytic dye degradation due to a shortening of the charge carrier lifetimes. So it may be expected that doping with a combination of Fe^{3+} and Cr^{3+} also may decrease the photocatalytic activity of TiO_2.

The undoped anatase sample nos. 2–4 and the anatase-rutile heterostructure, no. 6, will accelerate the polymerisation of the acrylate 1. The polymerisation rate as well as the conversion after 120 s illumination increase with increasing number of grain boundaries per secondary particle (see curves 2–4 in Fig. 4).

The highest polymerisation rate is observed for P25 due to its anatase-rutile heterojunction enhancing the charge separation as well as its high BET surface area.

The results indicate comparable trends in the case of the photopolymerisation as well as the photocatalytic degradation of organic compounds [9].

The polymerisation rate should increase with increasing U_{max} because this is a measure of the charge separation and it should increase with increasing BET surface area because it is a surface reaction. But with the exception of sample no. 6 U_{max} increases with decreasing BET surface area.

Fig. 5 shows the relation between the maximum Photo-EMF U_{max} and the maximum polymerisation rate r_P^{max} as well as the conversion C_{120s} of double bonds after 120 s illumination.

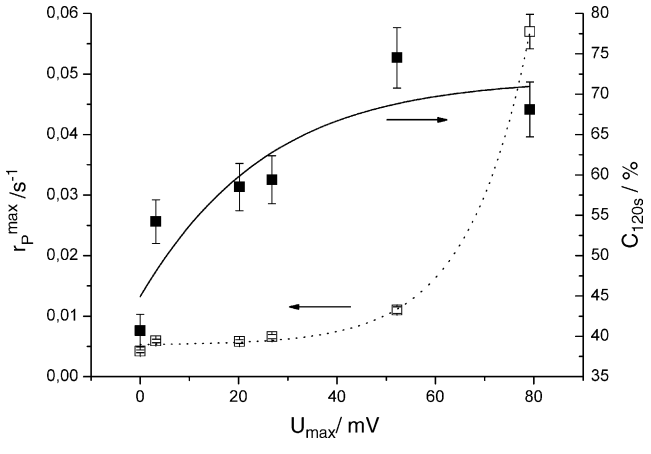

Fig. 5. Dependence of the maximum photopolymerisation rate r_P^{max} and the double bond conversion C_{120s} after an illumination time of 120 s on the maximum Photo EMF U_{max} for the TiO_2 photocatalysts nos. 1–6.

Fig. 5 proofs that for the anatase samples the polymerisation rate increases only slightly with increasing U_{max}. This is because the positive influence of an enhanced charge separation is partially compensated by the decrease of the BET surface area. In the case of the anatase-rutile heterostructure, sample no.6, a good charge separation due to the heterojunction is combined with a high BET surface area resulting in a much higher polymerisation rate.

So the results show that the photoelectric properties as well as the surface area of a photocatalyst material are important for its photocatalytic activity.

4. Conclusions

The rate of the photopolymerisation of an ethoxylated trisacrylate pigmented with TiO_2 strongly depends on the properties of the TiO_2 particles. Amorphous TiO_2 is not able to initiate the photopolymerisation of the acrylate. In contrast to this, in the presence of an anatase pigment a reasonable rate r_P^{max} of the photopolymerisation of the acrylate may be observed. Using pure undoped anatase the photopolymerisation rate of the acrylate increases with increasing average number of grain boundaries per secondary particle because grain boundaries enhance the charge separation. But with increasing number of grain boundaries per secondary particle the BET surface area decreases. For that reason the positive influence of the grain boundaries on the photopolymerisation rate is partially compensated by decreasing BET surface area.

The highest polymerisation rate was observed using the anatase-rutile heterostructure P25. The reasons for that are an improved charge separation by the heterojunction in combination with a large BET surface area.

Photo-EMF measurements of the TiO_2 photocatalyst materials allow an interpretation of the results of the polymerisation experiments.

A photocatalytic reaction is only possible if illumination leads to the generation of free charge carriers (hole/electrons) within the catalyst. For that reason the occurance of a Photo-EMF is a necessary condition for photocatalytic activity of a pigment.

A correlation between the maximum Photo-EMF and the acrylate polymerisation rate of crystalline TiO_2 pigments was observed. Thus, the photocatalytic activity increases with in-

creasing over all efficiency of charge formation and separation.

Generally, our results show that besides the BET surface area the photoelectric properties of the catalyst materials govern the photocatalytic activities. Measurements of the transient Photo-EMF are a useful tool to evaluate the photocatalytic activity of a material. For that reason photocatalytic reactions always should be investigated in combination with Photo-EMF measurements.

Acknowledgements

This work was financially supported by the german research foundation (DFG) and the Martin-Luther-University of Halle-Wittenberg. The authors would like to thank Prof. R. Mehnert and Dr. T. Scherzer (Institut für Oberflächenmodifizierung Leipzig) for the opportunity to perform time resolved IR spectroscopic investigations. Moreover, the authors acknowledge Dr. Th. Müller and Mrs. Lindner from the Department of Inorganic Chemistry of the University Halle for doing the XRD and the BET investigations, respectively. Furthermore, the authors thank Prof. R. Böttcher from the University of Leipzig for performing solid state EPR experiments and Dr. Poellmann from the Geographic Institute of the University of Halle-Wittenberg for doing X-ray fluorescence analysis.

References

[1] D.A. Tryk, A. Fujishima, K. Honda, Electrochim. Acta 45 (2000) 2363.
[2] A. Fujishima, K. Hashimoto, T. Watanabe, TiO_2 Photocatalysis, Fundamentals and Applications, Bkc Inc., Tokyo, 1999.
[3] N. Serpone, E. Pelizzetti (Eds.), Photocatalysis, Fundamentals and Applications, Wiley, New York, 1989.
[4] D.F. Ollis, H. Al-Ekabi (Eds.), Photocatalytic Purification and Treatment of Water and Air, Elsevier, Amsterdam, 1993.
[5] E. Pelizzetti, M. Schiavello (Eds.), Photochemical Conversion and Storage of Solar Energy, Kluwer Academic Publishers, Dordrecht, 1991.
[6] D.W. Bahnemann, Nachr. Chem. Tech. Lab. 42 (1994) 378.
[7] T. Minabe, D.A. Tryk, P. Sawunyama, Y. Kikuchi, K. Hashimoto, A. Fujishima, J. Photochem. Photobiol. A: Chem. 137 (2000) 53.
[8] S. Sakthivel, H. Kisch, Chem. Phys. Chem. 4 (2003) 487.
[9] C.H. Cho, D.K. Kim, J. Am. Ceram. Soc. 86 (7) (2003) 1138.
[10] W. Macyk, H. Kisch, Chem. Eur. J. 7 (9) (2001) 1862.
[11] D.W. Bahnemann, Isr. J. Chem. 33 (1993) 115.
[12] J. Laubrich, G. Israel, J. Inform. Rec. 24 (1998) 427.
[13] I.M. Arabatzis, T. Stergiopoulos, M.C. Bernard, L. Labou, S.G. Neophytides, P. Falares, Appl. Catal. B: Environ. 42 (2003) 187.
[14] C. Paulus, K. Wilke, H.D. Breuer, J. Inform. Rec. 24 (1998) 299.
[15] K. Wilke, H.D. Breuer, J. Inform. Rec. 24 (1998) 309.
[16] K. Wilke, H.D. Breuer, J. Photochem. Photobiol. A: Chem. 121 (1999) 49.
[17] J. Yu, X. Zhao, Q. Zhao, Mater. Chem. Phys. 69 (2001) 25.
[18] Z. Guan, X. Zhang, Y. Ma, Y. Cao, J. Yao, J. Mater. Res. 16 (4) (2001) 907.
[19] M.A. Maatoug, P. Anna, G. Bertalan, I. Kavadits, G. Marosi, I. Csontos, A. Marton, A. Toth, Macromol. Mater. Eng. 282 (2000) 30.
[20] U. Gesenhues, J. Photochem. Photobiol. A: Chem. 139 (2001) 243.
[21] M. Schiller, F.W. Mueller, C. Damm, J. Photochem. Photobiol. A: Chem. 149 (2002) 227.
[22] H. Kisch, H. Weiß, Adv. Funct. Mater. 12 (8) (2002) 483.
[23] H. Kisch, Adv. Photochem. 26 (2001) 93.
[24] K. Rosche, C. Decker, G. Israel, J.-P. Fouassier, Eur Polym. J. 33 (6) (1997) 849.
[25] A.J. Hoffman, H. Yee, G. Mills, M.R. Hoffmann, J. Phys. Chem. 96 (1992) 5540, 5546.
[26] I.R. Bellobono, R. Morelli, C.M. Chiodaroli, J. Photochem. Photobiol. A: Chem. 105 (1997) 89.
[27] I.G. Popovic, L. Katsikas, H. Weller, Pol. Bull. 32 (1994) 597.
[28] Z.Y. Huang, T. Barber, G. Mills, M.-B. Morris, J. Phys. Chem. 98 (1994) 12746.
[29] A. Troupis, A. Hiska, E. Papaconstaninou, Appl. Catal. B: Environ. 42 (2003) 305.
[30] K. Rajeshwar, C.R. Chentamarakshan, Y. Ming, W. Sun, J. Electroanal. Chem. 538–539 (2002) 173.
[31] M.I. Litter, Appl. Catal. B: Environ. 23 (1999) 89.
[32] B. Ohtani, Y. Ogawa, S.I.J. Nishimoto, J. Phys. Chem. B 101 (1997) 3746.
[33] K. Tanaka, M.F.V. Lapule, T. Hisanaga, Chem. Phys. Lett. 187 (1991) 73.
[34] S. Ruan, F. Wu, T. Zhang, W. Gao, B. Xu, M. Zhao, Mater. Chem. Phys. 69 (2001) 7.
[35] C. Damm, F.W. Mueller, G. Israel, H.P. Abicht, Dyes Pigments 56 (2003) 151.
[36] G. Israel, F.W. Mueller, C. Damm, J. Harenburg, J. Inform. Rec. 23 (1997) 559.
[37] F.W. Mueller, C. Damm, G. Israel, J. Inform. Rec. 25 (2000) 533.
[38] S. Gablenz, D. Voeltzke, H.P. Abicht, J. Neumann-Zdralek, J. Mater. Sci. Lett. 17 (1998) 537.